

Ultrathin Plasma Polymer Passivation of Perovskite Solar Cells for Improved Stability and Reproducibility

Jose M. Obrero-Perez, Lidia Contreras-Bernal,* Fernando Nuñez-Galvez, Javier Castillo-Seoane, Karen Valadez-Villalobos, Francisco J. Aparicio, Juan A. Anta, Ana Borrás, Juan R. Sanchez-Valencia, and Angel Barranco*

Despite the youthfulness of hybrid halide perovskite solar cells, their efficiencies are currently comparable to commercial silicon and have surpassed quantum-dots solar cells. Yet, the scalability of these devices is a challenge due to their low reproducibility and stability under environmental conditions. However, the techniques reported to date to tackle such issues recurrently involve the use of solvent methods that would further complicate their transfer to industry. Herein a reliable alternative relating in the implementation of an ultrathin plasma polymer as a passivation interface between the electron transport layer and the hybrid perovskite layer is presented. Such a nanoengineered interface provides solar devices with increased long-term stability under ambient conditions. Thus, without involving any additional encapsulation step, the cells retain more than 80% of their efficiency after being exposed to the ambient atmosphere for more than 1000 h. Moreover, this plasma polymer passivation strategy significantly improves the coverage of the mesoporous scaffold by the perovskite layer, providing the solar cells with enhanced performance, with a champion efficiency of 19.2%, a remarkable value for Li-free standard mesoporous n-i-p architectures, as well as significantly improved reproducibility.

1. Introduction

Under the scenario of the climate crisis caused by human actions,^[1,2] the photovoltaic field has undergone rapid progress in the last few years due to the development of solar devices based on hybrid metal halide perovskite materials.^[3] Currently, these devices have already achieved competitive efficiency as commercial silicon cells.^[4] To date, the most highly efficient perovskite solar cells (PSCs) have been achieved by mesoscopic architecture using mesoporous TiO₂ (*m*-TiO₂) as electron transport layer (ETL). The mesoporous scaffold is usually doped with hygroscopic compounds such as lithium salt to enhance its electron mobility.^[5–8] Although Li-treatment increases the performance of perovskite devices as it improves mainly the open-circuit voltage and fill factor of the cells, it also causes greater instability of the solar devices against ambient moisture

as well as low reproducibility of their photovoltaic parameters.^[9,10] Indeed, some of the most important bottlenecks to overcome nowadays for the practical exploitation of the PSCs are not related to record efficiency but to both: 1) their lack of reproducible fabrication approaches; and 2) inherent low stability under realistic outdoor conditions (moisture, UV illumination, temperature, etc.). In the first case, the dispersion in efficiency for PSCs is far from narrow in the more acknowledged laboratories, as it has been thoroughly discussed in reference articles on the topic as Saliba et al.,^[9] Jimenez-López et al.,^[11] Qiu et al.^[12] and many others. In the second place, the PSCs sensitivity to environmental conditions, especially of perovskite material, imposes the use of a dry atmosphere glove-box which hampers the large-scale production of these solar devices.^[13–18] In this context, numerous researchers have focused on finding passivation materials to modify interlayers that are not detrimental to the performance of the devices but that increase their stability. So far, the materials employed to passivate interfaces include 2D perovskites, metal oxide compounds, or insulating organic materials. These reported approaches typically use solutions methods, however, no alternative vacuum processes scalable to industrial manufacturing have been explored.^[19–21]


J. M. Obrero-Perez, L. Contreras-Bernal, F. Nuñez-Galvez, J. Castillo-Seoane, F. J. Aparicio, A. Borrás, J. R. Sanchez-Valencia, A. Barranco

Instituto de Ciencia de Materiales de Sevilla (CSIC-Universidad de Sevilla)
C/Americo Vespucio 49, Seville E-41092, Spain

E-mail: lidia.contreras@icmse.csic.es; angel.barranco@csic.es

K. Valadez-Villalobos, J. A. Anta
Departamento de Sistemas Físicos
Químicos y Naturales
Universidad Pablo de Olavide
Seville E-41013, Spain

F. J. Aparicio
Departamento de Física Aplicada I
Escuela Politécnica Superior
Universidad de Sevilla
c/ Virgen de África 7, Seville E-41011, Spain

 The ORCID identification number(s) for the author(s) of this article can be found under <https://doi.org/10.1002/aenm.202200812>.

© 2022 The Authors. Advanced Energy Materials published by Wiley-VCH GmbH. This is an open access article under the terms of the Creative Commons Attribution-NonCommercial-NoDerivs License, which permits use and distribution in any medium, provided the original work is properly cited, the use is non-commercial and no modifications or adaptations are made.

DOI: 10.1002/aenm.202200812

In this work, we propose the use of ultrathin plasma polymers as passivating material for the ETL/perovskite interface. These plasma polymeric films have already been successfully tested as encapsulating material for protecting PSC against water and moisture and also as conformal protective layers for organic supported nanostructures.^[22,23] The reported plasma polymerization technique is solventless, environmentally friendly, and fully compatible with large-scale fabrication.^[24] It is worth highlighting the fact that the same material fulfills different functions in the cell (water protection as an encapsulant and as a nanometric interface coating to modify and improve the cell behavior) could be a practical advantage that can help on the way to the industrially viable production of perovskite cells.

Here, the plasma films are grown in a single step by remote plasma assisted vacuum deposition (RPAVD) of adamantane powder.^[23,25] This molecule is a cage-like hydrocarbon consisting of sp^3 C–C bonds with the same spatial distribution that the C atoms in the diamond crystal, which is vacuum sublimated in presence of low-power remote microwave plasma. Applying this method, adamantane-based ultrathin plasma polymers were deposited at room temperature on the mesoporous titanium oxide (m -TiO₂/ADA) without any required pretreatment. Their microstructural characteristics have been observed by scanning electron microscopy (SEM). The plasma polymer resulting from this process is highly conformal, homogenous, compact and chemically inert, as we have already shown in our previous works.^[22,23] In addition, the ADA films are fully stable in air and thermally stable up to 250 °C in air. The photovoltaic behavior of the resulting solar cells has been analyzed under solar illumination conditions. To confirm the improvement of the reproducibility of PSCs incorporating the ADA layer, a statistical analysis has been performed for 20 devices of each configuration, including three different batches prepared along 3–4 months. Besides, the electronic effect of ADA polymeric passivation interface has been studied by electrochemical impedance and photoluminescence measurements.

The long-term stability under ambient conditions has been also analyzed and compared with those without ADA plasma polymeric passivation. To our best knowledge, this is the first reported work in which ultrathin plasma polymers are used at ETL/perovskite interface for PSC.

2. Results and Discussion

2.1. Adamantane Plasma Polymers on Mesoporous TiO₂ Electrode

A set of adamantane plasma polymer layers with different thicknesses has been tested as a passivation layer at m -TiO₂/perovskite interface for conventional n-i-p PSCs. These ADA films were deposited on top of the mesoporous TiO₂ layer using the remote plasma assisted vacuum deposition (RPAVD) reported in a previous work.^[22,23] A simplified schematic of the deposition process is shown in **Figure 1a**. In particular, ADA nanocomposite films of ca. 1, 5, and 15 nm (hereinafter referred to as ADA-1 nm, ADA-5 nm, and ADA-15 nm, respectively) have been prepared. The thickness of every ADA layer has been in situ monitored during deposition using a Quartz Crystal Mon-

itor (see experimental section in Supporting Information).^[26] In addition, the thickness was verified by Variable-Angle Ellipsometric Spectroscopy (VASE), whose spectra were fitted assuming a Cauchy model. The optical constant of the model, as well as the thickness, are shown in Table S1, Supporting Information. The cross-section SEM image of the thicker ADA film (m -TiO₂/ADA-15 nm) displays the characteristic morphology of a plasma polymer, forming a compact and conformal layer on top of the m -TiO₂ (see Figure S1, Supporting Information).

2.2. m -TiO₂/ADA as Electron Selective Contact in Perovskite Solar Cells

Figure 1a shows a schematic diagram of the device manufacturing process for solar devices based on m -TiO₂/ADA electrodes: using these electrodes as the ETL, the configuration of the solar device was completed with RbCsMAFA perovskite [(FAPbI₃)₈₃(MAPbBr₃)₁₇ + 5% CsI] + 5% RbI as the active layer and Spiro-OMeTAD as the hole transport layer (HTL) (see the Experimental Section for further details).^[9] m -TiO₂ electrodes without ADA films were used as reference samples (ADA-0 nm). Since deposited ADA films are partly hydrophobic,^[22] the perovskite solution does not wet the m -TiO₂/ADA samples. Thus, to achieve the full and homogeneous distribution of the perovskite film it was necessary to apply a short ozone treatment (hereafter UV/O₃ treatment) for 5 min to decrease the contact angle of the m -TiO₂/ADA surface (see Figure S2, Supporting Information). On these partially hydrophilic surfaces, the perovskite is optimally distributed. The UV/O₃ treatment hardly affected the surface composition of the polymer layer as seen by X-ray photoelectron spectroscopy (XPS) analysis. In particular, only the C1s X-ray photoelectron spectroscopy (XPS) peak revealed a slight increase in the contribution of carboxyl groups shown at higher binding energies (Figure 1b). It is also worth highlighting that the UV/O₃ treatment does not produce a significant decrease in the ADA thickness, as was verified by Variable-Angle Ellipsometric Spectroscopy (VASE) measurements (see Table S1, Supporting Information).

The perovskite film deposited on m -TiO₂/ADA electrodes was analyzed by SEM. Figure S3, Supporting Information, shows the images taken at the perovskite surface, from which can be observed two families of grain for all cases. ADA-0 nm shows the biggest grain size, while ADA samples have a higher homogeneity. Cross-sectional SEM images of each cell configuration are shown in **Figure 2**. In all cases, the devices exhibit a conventional profile in which the perovskite layers present large and well-defined grains and a thickness of \approx 600 nm (\approx 150 nm of m -TiO₂). We found that the mesoporous particles of TiO₂ were less visible in the case of ADA film was incorporated into the architecture. This effect can be attributed to a better coating of the m -TiO₂ by the perovskite layer. It is important to remark here that the only experimental difference between reference and ADA samples is the adamantane layer deposition step. In order to discard the possible effect of the plasma on the surface of the m -TiO₂, the reference samples were exposed to similar plasma conditions than for ADA preparation, but without the introduction of the adamantane precursor in the reaction chamber. After the synthesis of the perovskite layer on top, no variation with respect to the reference cells was observed

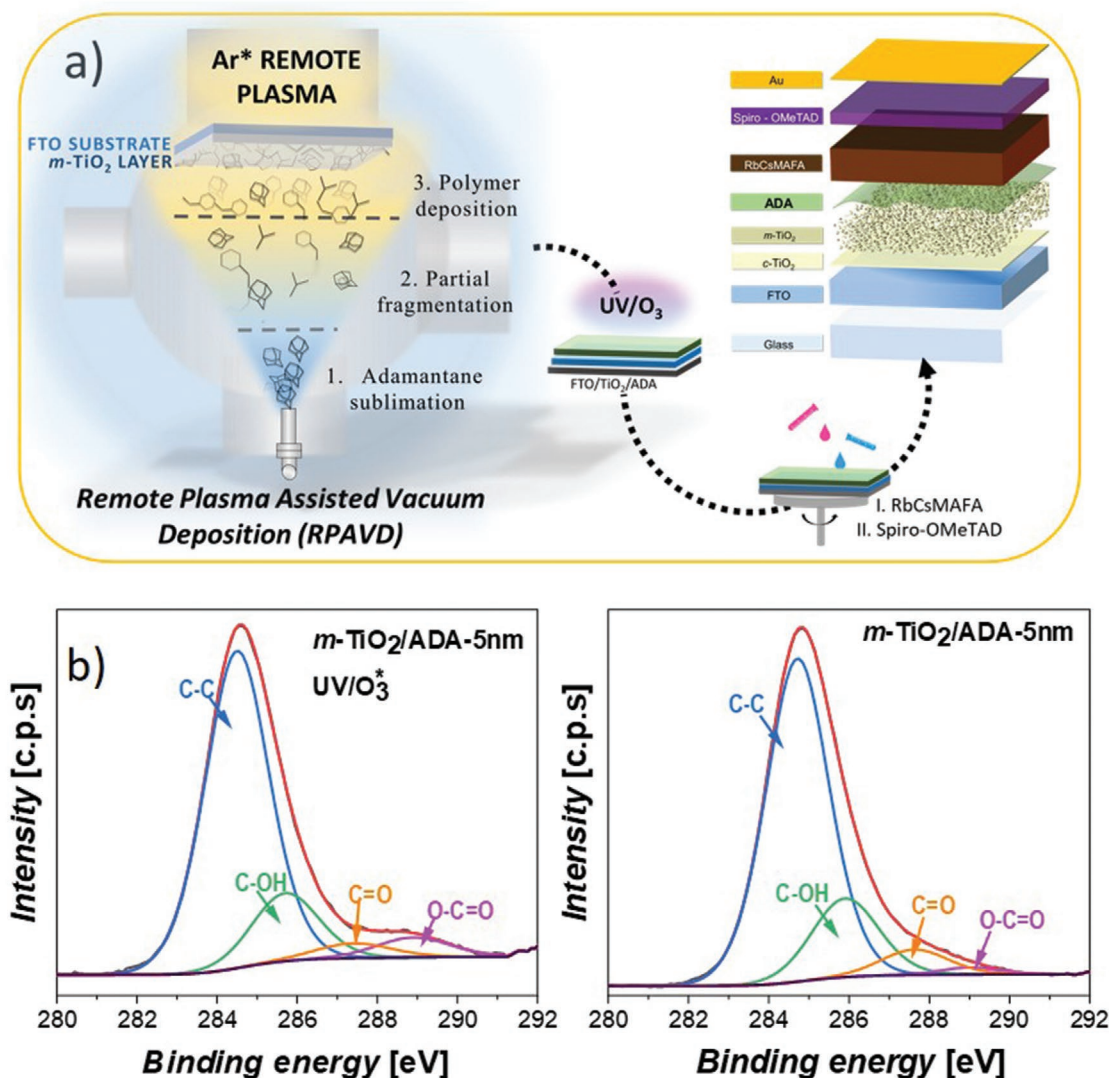


Figure 1. a) Schematic of the solar cell preparation process for devices based on $m\text{-TiO}_2/\text{ADA}$ electrodes. b) C 1s XPS peaks after and before the UV/O_3 surface activation treatment of the $m\text{-TiO}_2/\text{ADA}$ -5 nm surface.

in the microstructure of mesoporous scaffold or in the photovoltaic parameters of the resulting solar cells. Bearing this in mind, the better coating of $m\text{-TiO}_2$ by the perovskite material in the presence of the ADA interlayer can be attributed to the conformal deposition of this polymeric film. However, local defocusing cannot be fully ruled out as an inductor of microstructural differences observed due to the different dielectric properties of the ADA layer.

In particular, the best coverage at the $m\text{-TiO}_2$ /perovskite interface came from the ADA-5 nm sample. This would indicate that the ADA interface is beneficial for improving the contact between the ETL and the perovskite. This key feature would lead to higher charge injection and transport, and hence to a better performance of the whole device.

Figure 3a displays the current density–voltage curves (J – V curves) of the solar devices for the different studied ADA cells and references without ADA film measured under 1sun – AM 1.5G illumination. The champion efficiency of 19.2%

is obtained for ADA-5 nm devices compared to 18.2% for ADA-0 nm samples. As it can be seen in Figure 3b–e, the ADA interlayers increase not only the power conversion efficiency (PCE) (Figure 3e) but also the rest of the photovoltaic parameters of the device: open-circuit photovoltage (V_{OC}) (b), short-circuit photocurrent density (J_{SC}) (c), and fill Factor (d). A significant improvement in the reproducibility of ADA samples is also observed through testing 20 samples of each configuration (Figure 3b–e and Table S2, Supporting Information). It needs to be remarked here that such a high amount of samples have been prepared in three different batches (for both references and ADA layers), separated more than one month from each other. Despite the batch to batch reproducibility in PSCs is usually very low as reported by other authors, we have tested different batches to have a more representative sampling. It is worthy to mention that this statistical analysis is crucial to unravel the effect of the adamantane-based plasma polymer as an interlayer due to the reported low reproducibility of PSCs.

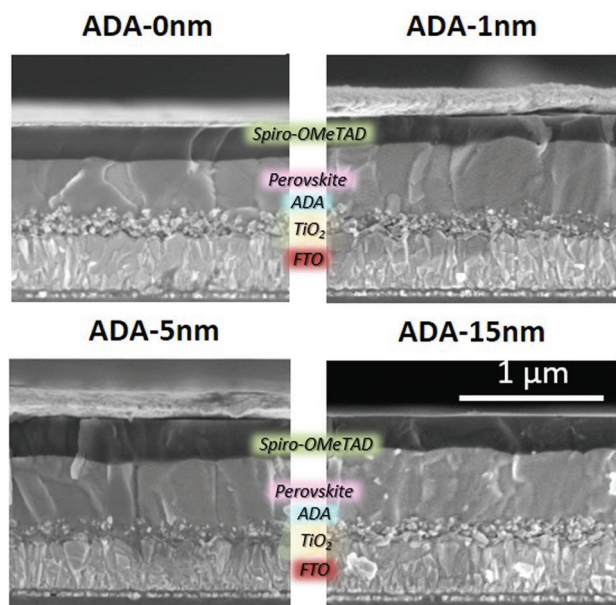


Figure 2. Cross-sectional SEM micrographs of complete perovskite solar cells with and without ADA polymer at the *m*-TiO₂/perovskite interface as labeled.

As a result of the statistical analysis, a significant increase of V_{OC} was found for ADA-5 nm and ADA-15 nm, that is, for samples with a polymer thickness greater than or equal to 5 nm (Figure 3b). In particular, the highest value was obtained for ADA-5 nm showing a champion V_{OC} of 1.15 V. In the case of J_{SC} , significant differences were found only for ADA layers above 15 nm (Figure 3c). ADA-15 nm showed the highest J_{SC} data of 23.1 mA cm⁻² versus the 22.5 mA cm⁻² measured for the reference sample. On the other hand, the highest impact of ADA polymer was observed in the FF parameter (Figure 3d). The best values of FF were achieved for the thickest ADA layers, with ADA-5 nm having a champion value of 79%. It is also important to stress herein that such a high fill factor is remarkable for TiO₂ ETL without Li-ions doping. In this context, the highest PCEs were obtained for ADA-5 nm samples (Figure 3e and Table S2, Supporting Information).

Interestingly, the ADA polymer acts as a passivation interlayer that positively impacts the hysteresis of J - V curves as well (Figures 3f and Figure S4, Supporting Information). The addition of a thin layer of the adamantane polymer at the interface reduces the hysteresis index, HI,^[27] by more than half (i.e., an average HI ≈0.13 and ≈0.05 for reference and ADA-5 nm, respectively).

To cast some light on this effect, electrochemical impedance spectroscopy (EIS) measurements at open-circuit voltage were carried out, as shown in Figure 4. We used a red LED ($\lambda = 635$ nm) as illumination source to ensure that the photo-generated charges are uniformly distributed inside the perovskite layer. This technique allows for discerning the electronic processes that happen at different frequencies.^[28–30] The impedance spectrum for a PSC is characterized by the presence of two signals: one at high frequency (HF, 10⁶–10³ Hz) and the other at low frequency (LF, <10 Hz). It is generally accepted that electronic transport and recombination processes affect mostly

the HF signal while the low one is related to ionic accumulation and migration.^[27,31–33] For this reason, we focus on the study of the first region. Well-defined arcs were observed in the HF region determined from the Nyquist plots from all samples as is typically the case for PSC (Figure 4a). For samples ADA-5 nm and ADA-15 nm, a lower onset of the Nyquist plots at high frequencies was found, indicating a lower series resistance (R_s) for these devices. This can be attributed to a better electronic transfer across the TiO₂/perovskite interface, consistent with the improved perovskite coverage mentioned above.

EIS plots were fitted by means of a simplified Voigt circuit (shown in Figure 4a) to extract the recombination resistance and geometrical capacitance associated with the high-frequency signal (R_{HF} and C_{HF} , respectively). We found that the R_{HF} values varied exponentially with the open-circuit potential from increased illumination light intensity, as predicted by the following equation:^[28,32]

$$R_{HF} = \left(\frac{\partial J_{rec}}{\partial V} \right)^{-1} = R_{00} \exp \left(- \frac{\beta q V}{k_B T} \right) \quad (1)$$

where J_{rec} is the recombination current, V is the photovoltage, R_{00} is the resistance at zero potential, β is the recombination parameter, k_B is the Boltzmann constant, and T is the absolute temperature. Figure 4b shows R_{HF} plot from which no significant change is inferred in the recombination resistance rates. However slight changes in slope (β) were observed (see Table S3, Supporting Information). According to previous works, the change in the β parameter suggests a different main recombination mechanism inside of the PSC, although some ionic effects cannot be ruled out.^[29,34] On the other hand, Figure S5, Supporting Information, shows that the high-frequency capacitance is also not significantly altered by the presence of Adamantane interlayer.

The charge collection efficiency (CCE) in the solar devices can be also estimated from EIS measures following the Equation (2):^[29,35,36]

$$CCE \approx \left(1 - \frac{R_{HF}(OC)}{R_{HF}(NOC)} \right) \times 100 \quad (2)$$

where R_{HF} is the high-frequency recombination resistance under open circuit (OC) and non-open circuit (NOC) conditions as defined by Equation (1). Table S4, Supporting Information, shows the CCE obtained for ADA and reference samples. We found that the CCE follows the following trend: ADA-5 nm > ADA-15 nm > ADA-0 nm. Bearing in mind that the CCE can be compared with the direct measurement of internal quantum efficiency,^[29,36] we can assume that the ADA interlayer induces a beneficial effect on charge transport dynamics.

On the other hand, EIS analyses were carried out to unravel the effect of the ultrathin ADA interlayer on the electronic properties of the *m*-TiO₂ material. For this purpose, dye-sensitized solar cells (DSSCs) based on thicker *m*-TiO₂/ADA electrodes were prepared, that is, ADA-5 nm and ADA-15 nm and ADA-0 nm as reference (see Experimental Section for further details). It is reported that the capacitance measured

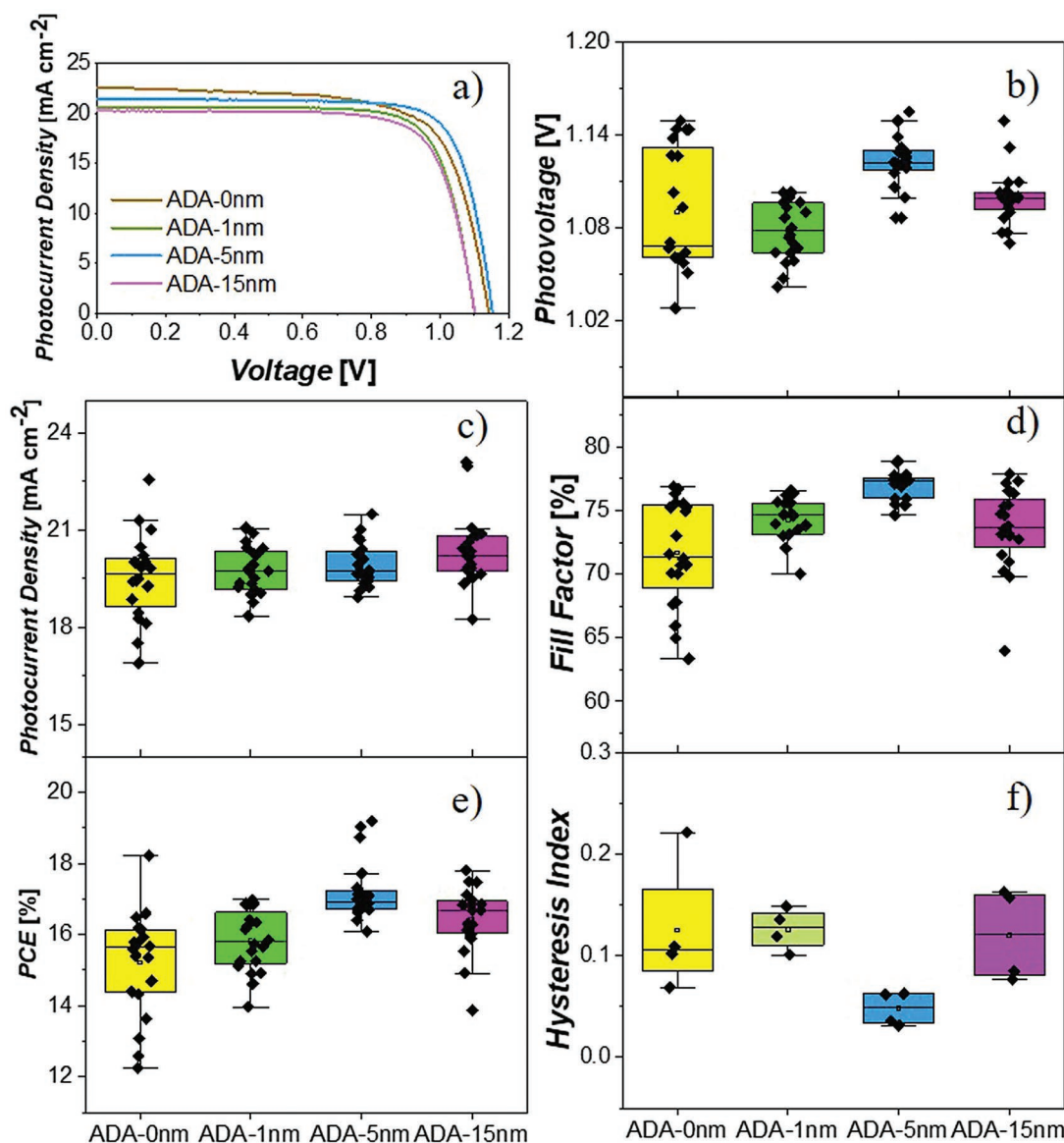


Figure 3. a) Current density–voltage curves of the champion cells of every type (ADA-0 nm, ADA-1 nm, ADA-5 nm, and ADA-15 nm). b–e) Photovoltaic parameters statistics acquired from 20 different devices for each configuration using analysis of variance. These data were recorded in reverse scans: b) open-circuit potential; c) photocurrent density; d) fill factor; and e) power conversion efficiency. f) Hysteresis index (HI) statistics obtained from 4 different devices for each configuration (see the Experimental Section for more details).^[27]

by EIS of DSSC based on TiO_2 electrodes corresponds to the trap energy distribution below the conduction band edge of this material.^[37–40] This capacitance, known as chemical capacitance (C_μ), shows an exponential variation with applied potential at open circuit conditions that is associated with a trapping distribution parameter (α) which ranges between 0.2–0.4 for TiO_2 -based DSSC. In this way, a change of C_μ , at a similar trap energy distribution value, indicates a shift in the conduction band edge.^[41] For example, this kind of variation can be observed by using electrolytes with different cation concentrations due to the interaction of the oxide with the surrounding electrolyte.^[42]

Figure 5a shows C_μ of our samples as a function of applied potential, obtained from fitting the Nyquist plots. In our case,

there are no differences in the C_μ between ADA samples and reference ones. Hence, the electronic properties of $m\text{-TiO}_2$ are not affected by the ADA passivation layer.

Figure 5b shows the photoluminescence (PL) spectra of perovskite deposited on $m\text{-TiO}_2$ layer passivated with ADA polymers (reference ADA-0 nm is also added). For a better comparison of intensity peak, PL data has been normalized to the absorbance at illumination wavelength (Figure S6, Supporting Information). In this way, it is possible to analyze the impact of the ADA polymer at the interlayer on both electron injection and light-harvesting.^[43] The figure shows a higher PL peak intensity for the reference than ADA samples. The lowest PL signal is observed for ADA-5 nm. Bearing in mind that the PL signal arises from the radiative recombination inside the

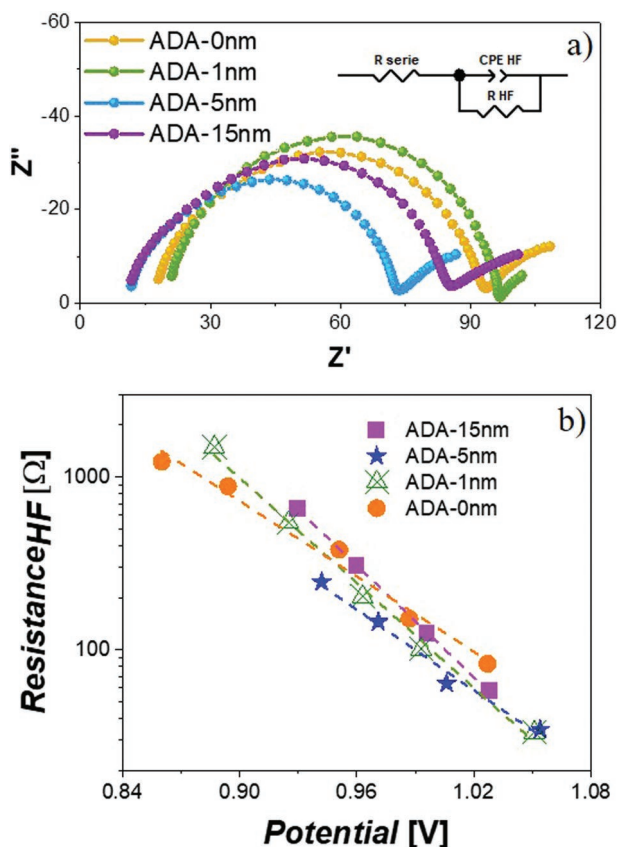


Figure 4. a) Nyquist plots obtained by impedance spectroscopy for ADA and reference samples (ADA-0 nm). These spectra were recorded at open circuit potential, with an applied voltage of 1.008 V using red light (LED) as the illumination source. b) Resistance element extracted from Nyquist plots using simple Voigt equivalent circuit fitting restricted to the high-frequency region.

perovskite film, a decreased PL intensity means faster electron injection from the perovskite layer into the TiO_2 layer.^[43] Therefore, a better electron transfer across the m - TiO_2 /perovskite interface is obtained when ADA was incorporated into

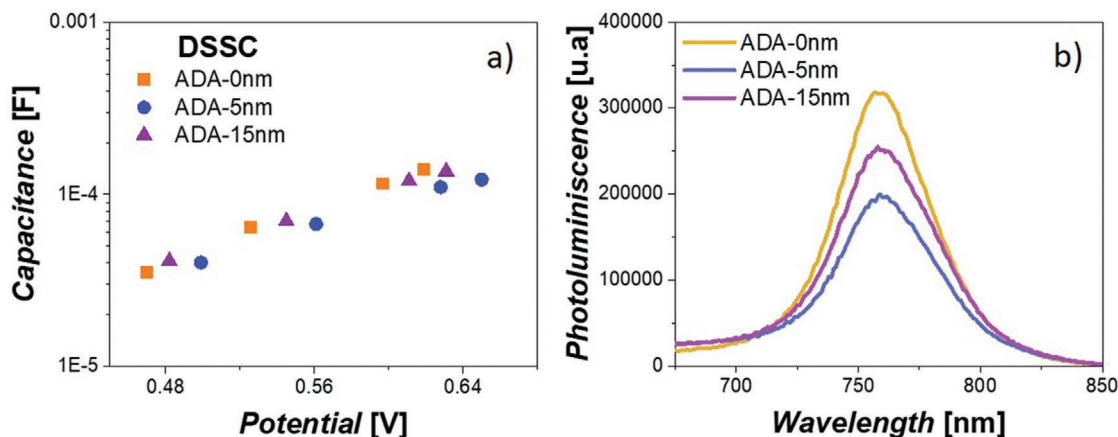


Figure 5. a) Chemical capacitance data extracted from impedance spectroscopy measurements for dye sensitized solar cells based on ADA samples. b) Steady-state photoluminescence spectra of perovskite deposited on mesoporous TiO_2 layer passivated ADA polymer. An excitation wavelength of 450 nm was used.

the structure, indicating that the ADA interlayer has a kinetic rather than a thermodynamic effect on PSCs.

2.3. Cell Stability

In a previous work, ADA films had been used as encapsulation material (with a significantly higher thickness) for solar cells to increase cell stability and resistance to moisture and water.^[22] This plasma-polymer is very stable against chemical and environmental agents.^[23] In this work, we have studied the long-term stability of the cells with ADA polymers at the m - TiO_2 /perovskite interface under dark conditions (test I, Figure 6a) and lighting cycles (test II, Figure 6b) both under ambient conditions ($\approx 50\%$ relative humidity and $\approx 23^\circ C$). First, samples were stored in air and dark for almost 300 h. Under test I, ADA-5 nm kept its initial PCE value until the end of the experiment while ADA-0 nm lost 15% of PCE after 150 h of storage (Figure 6a). Second, we also tested the stability of the devices under indoor lighting cycles for 9 h per day. Figure 6b shows the normalized PCE as a function of time for the PSCs under test II conditions. For test II, we recorded the PCE for longer than in test I (more than 1500 h) due to the samples stored in dark (test I) and the ones subjected to indoor lighting cycles (test II) showing similar stability during the first 200 h. Bearing in mind that our samples were not encapsulated, ADA-5 nm showed good stability after more than 1000 h showing a retaining of 80% of the original PCE. However, ADA-0 nm was significantly damaged after 1000 h of storage. Figure 6c shows the appearance of the samples under test II conditions for more than 2000 h. It is clearly noticeable how the ADA-5 nm sample shows no obvious signs of degradation while the reference sample appears completely degraded.

3. Conclusions

Ultrathin adamantane plasma-polymeric films have been incorporated to PSCs as passivation material at m - TiO_2 /perovskite interface. We have found that the ADA passivation interlayer results in devices with: 1) higher values for most of the

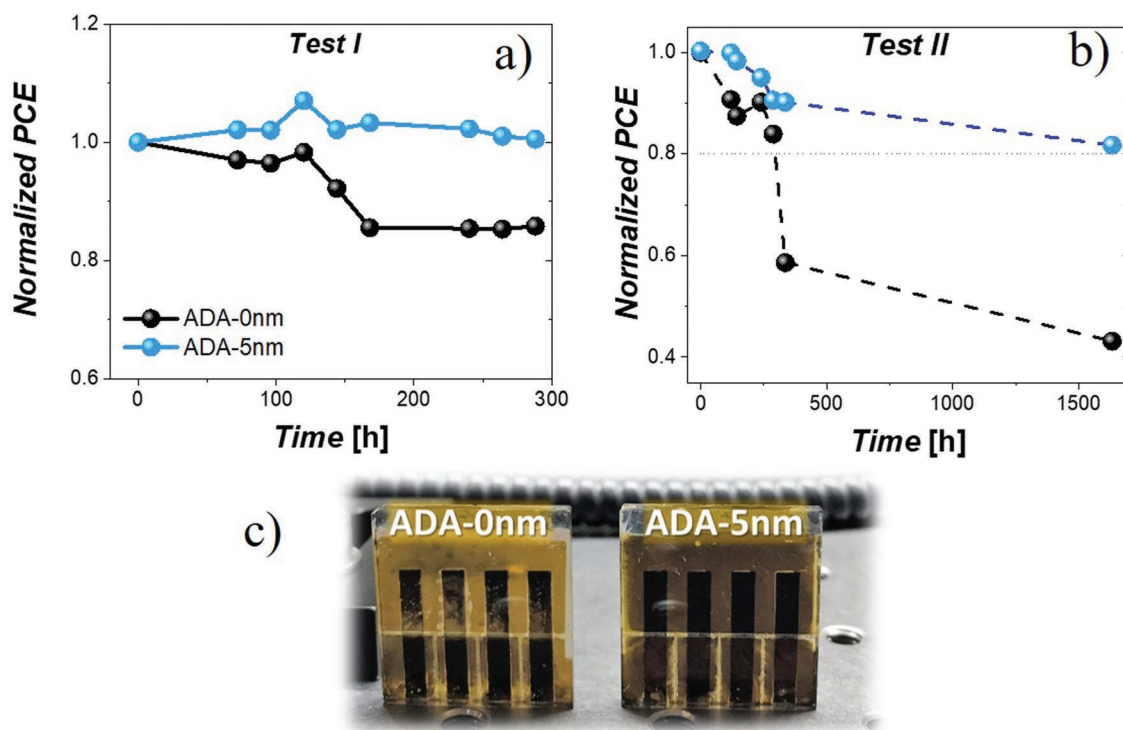


Figure 6. Normalized power conversion efficiency as a function of time measured under 1 sun – AM1.5G illumination in the reverse scan using a scan rate of 100 mV s^{-1} . The measurements were carried out at 50% relative humidity and $23 \text{ }^\circ\text{C}$ for samples stored under dark conditions (a) and for samples kept under indoor lighting cycles for 9 h per day (b). c) Photograph of the samples after more than 2000 h under test II conditions.

photovoltaic parameters than reference samples; 2) showing also huge improvement in the data reproducibility. In particular, ADA5-nm shows remarkable efficiency up to 19.2% and fill factor of 79%, taking into account that our devices are free of the TiO_2 lithium doping. Second, the photovoltaic data accuracy of ADA samples increased to more than 50%.

To confirm the improvement of the reproducibility of PSCs incorporating the ADA layer, a statistical analysis has been performed for 20 devices of each configuration, including three different batches prepared along 3–4 months.

The beneficial effect on fill factor seems to come from the drop of series resistance observed by EIS and the improvement of electron injection found in the PL measurements. In addition, since the photogenerated carriers are more efficiently injected into $m\text{-TiO}_2$ leading to the balance in the flux of charge transports, the hysteresis of the $J\text{-}V$ curve is also reduced by using $m\text{-TiO}_2/\text{ADA-5 nm}$ electrode. This is attributed to improved coverage of the mesoporous titanium particles by the perovskite, as has been observed in the SEM analysis of the devices. On the other hand, the EIS analysis of DSSC based on $m\text{-TiO}_2/\text{ADA}$ electrodes proves that the ADA treatment does not alter the electronic properties of the TiO_2 electrodes. From the analysis of our results, we can establish an optimum plasma-polymer thickness of 5 nm to maximize the performance. Finally, the ADA-5 nm samples show a significant stability increase under environmental conditions in comparison with the reference devices. ADA-5 nm samples, measured without encapsulation at ambient conditions, retained 80% of their initial efficiency in 1000 h.

Our results demonstrate the reliability of the plasma technique for PSCs interlayer passivation. The plasma polymer fabrication is carried out by a solvent-free process that can be applied to large areas and/or simultaneous deposition of multiple electrodes. This type of plasma-based deposition process can easily be scaled up for industrial manufacturing, which could help bring PSCs closer to commercialization. In addition, we have previously proved that the same material can be used to encapsulate the cells in a final step. The fact that the same material can fulfill different functions in the cell (water protection as an encapsulant and as a nanometric interface coating to improve the cell behavior) could be a practical advantage that can help on the way to the industrially viable production of perovskite cells.

Supporting Information

Supporting Information is available from the Wiley Online Library or from the author.

Acknowledgements

The authors thank projects PID2019-110430GB-C21, PID2019-110430GB-C22, and PID2019-109603RA-I00 funded by MCIN/AEI/10.13039/501100011033 and by “ERDF (FEDER) A way of making Europe”, by the “European Union”. They also thank the Consejería de Economía, Conocimiento, Empresas y Universidad de la Junta de Andalucía (PAIDI-2020 through projects US-1263142, US-1381057, P18-RT-3480), and the EU through

cohesion fund and FEDER 2014–2020 programs for financial support. J.R.S.-V. Thanks the University of Seville through the VI PPIT-US. L.C.B. acknowledges the “Juan de la Cierva” program funded by MCIN/AEI/10.13039/501100011033. F.J.A. also thanks the EMERGIA Junta de Andalucía program. J.A.A. thanks MCIN/AEI/10.13039/501100011033 for SCALEUP SOLAR-ERA.net project PCI2019-111839-2. The authors also thank the CSIC *Interdisciplinary Platform for Sustainable Plastics towards a Circular Economy* (PTI-SusPlast+). The project leading to this article has received funding from the EU H2020 program under grant agreement 851929 (ERC Starting Grant 3DScavengers).

Conflict of Interest

The authors declare no conflict of interest.

Data Availability Statement

The data that support the findings of this study are available from the corresponding author upon reasonable request.

Keywords

passivation interfaces, perovskite solar cells, plasma and vacuum deposition, stability, ultrathin polymers

Received: March 8, 2022

Revised: May 17, 2022

Published online: July 12, 2022

- [1] N. Oreskes, *Science* **2004**, *306*, 1686.
- [2] P. C. Jain, *Renewable Energy* **1993**, *3*, 403.
- [3] T. C. Sum, N. Mathews, *Energy Environ. Sci.* **2014**, *7*, 2518.
- [4] Best Research-Cell Efficiency Chart; <https://www.nrel.gov/pv/cell-efficiency.html> (accessed: May 2022).
- [5] E. Guillén, F. J. Ramos, J. A. Anta, S. Ahmad, *J. Phys. Chem. C* **2014**, *118*, 22913.
- [6] F. Giordano, A. Abate, J. P. Correa Baena, M. Saliba, T. Matsui, S. H. Im, S. M. Zakeeruddin, M. K. Nazeeruddin, A. Hagfeldt, M. Graetzel, *Nat. Commun.* **2016**, *7*, 10379.
- [7] M. Saliba, T. Matsui, K. Domanski, J.-Y. Seo, A. Ummadisingu, S. M. Zakeeruddin, J.-P. Correa-Baena, W. R. Tress, A. Abate, A. Hagfeldt, M. Graetzel, *Science* **2016**, *354*, 206.
- [8] A. D. Jodowski, C. Roldán-Carmona, G. Grancini, M. Salado, M. Ralairisoo, S. Ahmad, N. Koch, L. Camacho, G. de Miguel, M. K. Nazeeruddin, *Nat. Energy* **2017**, *2*, 972.
- [9] M. Saliba, J.-P. Correa-Baena, C. M. Wolff, M. Stolterfoht, N. Phung, S. Albrecht, D. Neher, A. Abate, *Chem. Mater.* **2018**, *30*, 4193.
- [10] J. Chung, S. S. Shin, G. Kim, N. J. Jeon, T.-Y. Yang, J. H. Noh, J. Seo, *Joule* **2019**, *3*, 1977.
- [11] J. Jiménez-López, B. M. D. Puscher, D. M. Guldi, E. Palomares, *J. Am. Chem. Soc.* **2020**, *142*, 1236.
- [12] L. Qiu, L. Chen, W.-H. Chen, Y. Yuan, L. Song, D. Mei, B. Bai, F. Xie, P. Du, J. Xiong, *ChemElectroChem* **2022**, *9*, 202101483.
- [13] B. Li, Y. Li, C. Zheng, D. Gao, W. Huang, *RSC Adv.* **2016**, *6*, 38079.
- [14] S. F. Lux, L. Terborg, O. Hachmöller, T. Placke, H.-W. Meyer, S. Passerini, M. Winter, S. Nowak, *J. Electrochem. Soc.* **2013**, *160*, A1694.
- [15] L. Qiu, L. K. Ono, Y. Qi, *Mater. Today Energy* **2018**, *7*, 169.
- [16] A. Abate, J.-P. Correa-Baena, M. Saliba, M. S. Su'ait, F. Bella, *Chem. – Eur. J.* **2018**, *24*, 3083.
- [17] M. Salado, L. Contreras-Bernal, L. Calio, A. Todinova, C. López-Santos, S. Ahmad, A. Borrás, J. Idígoras, J. A. Anta, *J. Mater. Chem. A* **2017**, *5*, 10917.
- [18] L. Contreras-Bernal, C. Aranda, M. Valles-Pelarda, T. T. Ngo, S. Ramos-Terrón, J. J. Gallardo, J. Navas, A. Guerrero, I. Mora-Seró, J. Idígoras, J. A. Anta, *J. Phys. Chem. C* **2018**, *122*, 5341.
- [19] A. A. Sutanto, P. Caprioglio, N. Drigo, Y. J. Hofstetter, I. Garcia-Benito, V. I. E. Queloz, D. Neher, M. K. Nazeeruddin, M. Stolterfoht, Y. Vaynzof, G. Grancini, *Chem* **2021**, *7*, 1903.
- [20] L. Zuo, H. Guo, D. W. deQuilettes, S. Jariwala, N. De Marco, S. Dong, R. DeBlock, D. S. Ginger, B. Dunn, M. Wang, Y. Yang, *Sci. Adv.* **2017**, *3*, e1700106.
- [21] Q. Wang, Q. Dong, T. Li, A. Gruverman, J. Huang, *Adv. Mater.* **2016**, *28*, 6734.
- [22] J. Idígoras, F. J. Aparicio, L. Contreras-Bernal, S. Ramos-Terrón, M. Alcaire, J. R. Sánchez-Valencia, A. Borrás, Á. Barranco, J. A. Anta, *ACS Appl. Mater. Interfaces* **2018**, *10*, 11587.
- [23] M. Alcaire, F. J. Aparicio, J. Obrero, C. López-Santos, F. J. Garcia-Garcia, J. R. Sánchez-Valencia, F. Frutos, K. (Ken) Ostrikov, A. Borrás, A. Barranco, *Adv. Funct. Mater.* **2019**, *29*, 1903535.
- [24] F. J. Aparicio, M. Holgado, A. Borrás, I. Blaszczyk-Lezak, A. Griol, C. A. Barrios, R. Casquel, F. J. Sanza, H. Sohlström, M. Antelius, A. R. González-Elipse, A. Barranco, *Adv. Mater.* **2011**, *23*, 761.
- [25] A. Barranco, P. Groening, *Langmuir* **2006**, *22*, 6719.
- [26] F. J. Aparicio, A. Borrás, I. Blaszczyk-Lezak, P. Gröning, A. Álvarez-Herrero, M. Fernández-Rodríguez, A. R. González-Elipse, A. Barranco, *Plasma Processes Polym.* **2009**, *6*, 17.
- [27] L. Contreras, J. Idígoras, A. Todinova, M. Salado, S. Kazim, S. Ahmad, J. A. Anta, *Phys. Chem. Chem. Phys.* **2016**, *18*, 31033.
- [28] L. Contreras-Bernal, M. Salado, A. Todinova, L. Calio, S. Ahmad, J. Idígoras, J. A. Anta, *J. Phys. Chem. C* **2017**, *121*, 9705.
- [29] L. Contreras-Bernal, S. Ramos-Terrón, A. Riquelme, P. P. Boix, J. Idígoras, I. Mora-Seró, J. A. Anta, *J. Mater. Chem. A* **2019**, *7*, 12191.
- [30] J. Idígoras, L. Contreras-Bernal, J. M. Cave, N. E. Courtier, Á. Barranco, A. Borrás, J. R. Sánchez-Valencia, J. A. Anta, A. B. Walker, *Adv. Mater. Interfaces* **2018**, *0*, 1801076.
- [31] A. Guerrero, G. Garcia-Belmonte, I. Mora-Sero, J. Bisquert, Y. S. Kang, T. J. Jacobsson, J.-P. Correa-Baena, A. Hagfeldt, *J. Phys. Chem. C* **2016**, *120*, 8023.
- [32] J.-P. Correa-Baena, M. Anaya, G. Lozano, W. Tress, K. Domanski, M. Saliba, T. Matsui, T. J. Jacobsson, M. E. Calvo, A. Abate, M. Grätzel, H. Míguez, A. Hagfeldt, *Adv. Mater.* **2016**, *28*, 5031.
- [33] E. J. Juárez-Perez, M. Wußler, F. Fabregat-Santiago, K. Lakus-Wollny, E. Mankel, T. Mayer, W. Jaegermann, I. Mora-Sero, *J. Phys. Chem. Lett.* **2014**, *5*, 680.
- [34] A. Castro-Chong, A. J. Riquelme, T. Aernouts, L. J. Bennett, G. Richardson, G. Oskam, J. A. Anta, *ChemPlusChem* **2021**, *86*, 1347.
- [35] A. Riquelme, F. E. Gálvez, L. Contreras-Bernal, H. Míguez, J. A. Anta, *J. Appl. Phys.* **2020**, *128*, 133103.
- [36] A. Riquelme, L. J. Bennett, N. E. Courtier, M. J. Wolf, L. Contreras-Bernal, A. B. Walker, G. Richardson, J. A. Anta, *Nanoscale* **2020**, *12*, 17385.
- [37] E. Guillén, L. M. Peter, J. A. Anta, *J. Phys. Chem. C* **2011**, *115*, 22622.
- [38] J. Bisquert, *J. Phys. Chem. B* **2004**, *108*, 2323.
- [39] J. Idígoras, G. Burdziński, J. Karolczak, J. Kubicki, G. Oskam, J. A. Anta, M. Ziótek, *J. Phys. Chem. C* **2015**, *119*, 3931.
- [40] S. R. Raga, E. M. Barea, F. Fabregat-Santiago, *J. Phys. Chem. Lett.* **2012**, *3*, 1629.
- [41] F. Fabregat-Santiago, J. Bisquert, G. Garcia-Belmonte, G. Boschloo, A. Hagfeldt, *Sol. Energy Mater. Sol. Cells* **2005**, *87*, 117.
- [42] D. F. Watson, G. J. Meyer, *Coord. Chem. Rev.* **2004**, *248*, 1391.
- [43] L. Contreras-Bernal, A. Riquelme, J. J. Gallardo, J. Navas, J. Idígoras, J. A. Anta, *ACS Sustainable Chem. Eng.* **2020**, *8*, 7132.